Talanta 308 (2026) 129885

Contents lists available at ScienceDirect

Talanta

journal homepage: www.elsevier.com/locate/talanta

# The multidimensional signature of oxysterols: Comparative RPLC-HRMS-based profiling of healthy and pancreatic tumour cell lines

Vito Nettis [a], Andrea Castellaneta [a,*], Noa Ndimurwanko [c,d], Francesco Greco [c,e], Valentina Casieri [f], Vincenzo Lionetti [f,g], Elisa Giovannetti [c,h], Liam A. McDonnell [c], Tommaso R.I. Cataldi [a,b], Cosima D. Calvano [a,b]

[a] Dipartimento di Chimica, Università degli Studi di Bari Aldo Moro, via Orabona 4, Bari, 70126, Italy
[b] Centro Interdipartimentale SMART, Università degli Studi di Bari Aldo Moro, via Orabona 4, Bari, 70126, Italy
[c] Fondazione Pisana per la Scienza ONLUS, San Giuliano Terme, 56017, Italy
[d] Scuola Normale Superiore, Pisa, 56126, Italy
[e] Fondazione Toscana Gabriele Monasterio, Pisa, 56124, Italy
[f] TrancriLab, Interdisciplinary Research Center "Health Science", Scuola Superiore Sant'Anna, Pisa, 56127, Italy
[g] UOSVD Anesthesia and Intensive Care, Fondazione Toscana G. Monasterio, Pisa, 56124, Italy
[h] Department of Medical Oncology, Cancer Center Amsterdam, VU University, Amsterdam, 1081 HV, the Netherlands

ARTICLE INFO

*Keywords:*
Oxysterols
Pancreatic cancer cells
Extracellular vesicles
Oxygen deprivation
High-resolution mass spectrometry
In-source fragmentation
Interplay of RPLC stationary phases

ABSTRACT

Oxysterols (OS) are emerging as active drivers of cancer, shaping aggressive, immunosuppressive tumour niches rather than acting as passive cholesterol byproducts. Here, we developed and applied an advanced LC–MS strategy for the comprehensive qualitative and quantitative profiling of the total (free and esterified) OS amount in healthy human pancreatic epithelial nestin-expressing (HPNE) cells and pancreatic ductal adenocarcinoma (PANC-1) cells. Both cell types were cultured under normoxic and hypoxic conditions to elucidate the impact of oxygen availability on OS metabolism.

OS separation was achieved using two complementary stationary phases, *i.e.*, cyanopropyl (ES-CN) and pentafluorophenyl (F5), providing orthogonal chromatographic selectivity. OS identification relied on retention matching with analytical standards across both columns and was further confirmed by the evaluation of diagnostic in-source fragmentation patterns. This multidimensional analytical framework ensured the unambiguous screening of up to 14 OS in cells and their extracellular vesicles (EVs). The tumour cell phenotype, together with hypoxic conditions, was associated with a marked accumulation of *ring-oxidized* OS, including 3β,5α,6β-cholestantriol, 7-ketocholesterol, and 7-hydroxycholesterol epimers, suggesting either a metabolic rewiring or an increased intracellular oxidative environment. In contrast, *side-chain* OS showed distinct dependencies on cell type and oxygen availability: 24(S)-hydroxycholesterol was reduced in tumour cells while the amount of 26(R/S)-hydroxycholesterol was increased when both cell types were grown in normoxic conditions. EVs exhibited a unique OS signature dominated by 25-hydroxycholesterol and 5β,6β-epoxycholesterol.

This study proposes a robust, orthogonal LC-MS workflow for OS profiling and provides new insights into the regulation of OS levels in pancreatic cancer, paving the way for future fundamental biochemical investigations.

## 1. Introduction

Cancer is the second leading cause of death worldwide. In 2022, 20 million new cases were reported, and this number is expected to rise over the next two decades [1,2]. Among all cancer types, pancreatic cancer (PC) ranks among the most aggressive and lethal malignancies. Due to its increasing incidence, it is projected that by 2030 PC will constitute the third leading cause of cancer-related mortality in Europe and the second in the United States [3,4]. PC typically originates in the ductal cells of the pancreas, with approximately 90% of cases being pancreatic ductal adenocarcinoma (PDAC) usually managed with chemotherapy in advanced stages. Still, chemotherapy has very limited efficacy, with a median overall survival of 6-12 months [5]. Indeed, PC remains asymptomatic in the early stages and has a grim prognosis with a 5-year overall survival rate of just 13% [6], mostly due to late

* Corresponding author.
*E-mail address:* andrea.castellaneta@uniba.it (A. Castellaneta).

https://doi.org/10.1016/j.talanta.2026.129885
Received 6 March 2026; Received in revised form 10 April 2026; Accepted 20 April 2026
Available online 21 April 2026
0039-9140/© 2026 The Authors. Published by Elsevier B.V. This is an open access article under the CC BY license (http://creativecommons.org/licenses/by/4.0/).

**List of recurring acronyms and abbreviations**

%RA – Relative Abundance
22(R)-HC – 22(R)-hydroxycholesterol
22(S)-HC – 22(S)-hydroxycholesterol
24(S)-HC – 24(S)-hydroxycholesterol
25-HC – 25-hydroxycholesterol
25(R)-26-HC – 25(R)-26-hydroxycholesterol
25(S)-26-HC – 25(S)-26-hydroxycholesterol
4β-HC – 4β-hydroxycholesterol
5α,6α-EC – 5α,6α-epoxycholesterol
5β,6β-EC – 5β,6β-epoxycholesterol
7α,25-HC – 7α-25-dihydroxycholesterol
7α-HC – 7α-hydroxycholesterol
7β-HC – 7β-hydroxycholesterol
7 KC – 7-ketocholesterol
CI – Confidence interval
CT – 3β,5α,6β-cholestantriol
d6-25-HC – Hexadeuterated 25-hydroxycholesterol
d7-5α,6α – Heptadeuterated-5α,6α-epoxycholesterol
EIC – Extracted Ion Chromatogram
(H)ESI – (Heated) ElectroSpray Ionization
ES-CN – Cyanopropyl stationary phase
EV(s) – Extracellular Vesicle(s)
F5 – Pentafluorophenyl stationary phase
FTMS – Fourier Transform (high-resolution) Mass Spectrometry
HPNE – Human Pancreatic Nestin-Expressing
NTA – Nano Tracking Analysis
OS – Oxysterol(s)
PANC1 – Human pancreatic ductal adenocarcinoma
PC – Pancreatic Cancer
PCA – Principal Component Analysis
PDAC – Pancreatic Ductal Adenocarcinoma
pNET – Pancreatic neuroendocrine tumour
RPLC – Reversed Phase Liquid Chromatography
ROS – Reactive Oxygen Species
WB – Western Blot

diagnosis. The effectiveness of laboratory-based tests for PC screening, such as the serum assay of carbohydrate antigen 19-9 [7] (CA 19-9), is limited by their generally low sensitivity and specificity [8]. Consequently, imaging modalities including endoscopic ultrasound and magnetic resonance imaging currently represent the most effective approaches for early diagnosis [9]. However, their use is largely restricted to individuals at high risk, such as those with genetic or hereditary predisposition, a positive family history, or the presence of established preneoplastic pancreatic lesions. For these reasons, considerable research efforts are currently focused on identifying novel biomarkers to improve early detection and to enhance monitoring of disease progression and therapy [10].

Fundamental studies on the metabolic dynamics of PC cells can contribute to the biomarker discovery process. Metabolic reprogramming plays a crucial role in PDAC to fulfil the energy and biomass requirements of tumour cell growth [11]. One crucial alteration is the upregulation of glycolysis, even under normoxic conditions (*Warburg effect*), which has been reported to increase steady-state reactive oxygen species (ROS) levels through decreasing the cell's antioxidant capacity [12]. Along with other biomolecules, lipids can be extensively targeted by ROS [13]. In particular, the ROS-mediated oxidation of cholesterol (one of the most abundant lipids in cell membranes [14]) primarily involves the carbon-carbon double bond and the labile allylic hydrogens [15,16], leading to the formation of specific oxysterols (OS), namely 7-ketocholesterol (7-KC), 7α-hydroxycholesterol (7α-HC), 7β-hydroxycholesterol (7β-HC), 5β,6β-epoxycholesterol (5β,6β-EC), 5α,6α-epoxycholesterol (5α,6α-EC), and 3β,5α,6β-cholestanetriol (CT) [16–18]. These are commonly referred to as *ring*-OS due to the presence of an additional oxygen-containing moiety on the rigid sterol ring system rather than on the side chain. The production of *side-chain* OS, including 26(R/S)-hydroxycholesterol (26(R/S)-HC), 24(S)-hydroxycholesterol (24(S)-HC), and 25-hydroxycholesterol (25-HC), is catalysed by specific enzymes and cannot be triggered by ROS [19,20].

Aside from being recognised as oxidative stress markers, 7-KC and 7β-HC have been postulated to play a role in the tumour microenvironment, where they modulate key cellular processes such as proliferation, migration and apoptosis [21–23]. Moreover, 7α-HC plasma levels have been reported to positively correlate with tumour size in patients with luminal-type breast cancer [24]. The role of 25-HC and 26-HC epimers was also investigated in the development of breast, ovarian, colon, liver, and bladder cancers [25–28].

Interestingly, two OS moieties have previously been reported in relation to PC. Among them, 5α,6α-EC was proposed as a potential biomarker in a study comparing serum samples from 40 patients diagnosed with PDAC and 40 healthy controls [29]. Soncini et al. [30] observed that CYP46A1, *i.e.*, the enzyme responsible for the conversion of cholesterol into 24(S)-HC, plays a role in the development of pancreatic neuroendocrine tumours (pNET), and that this role requires activation of HIF-1α [30]. Hypoxia is a central hallmark of PDAC; HIF-1α [30] is highly overexpressed in PDAC tissues, and the hypoxic microenvironment plays a critical role in the disease's resistance to treatment [31].

Building on this background, here we report the comprehensive characterisation of a large pool of OS in human PDAC cells (PANC-1) and healthy human pancreatic ductal cells (HPNE) grown in both normoxic and hypoxic conditions. The analytical characterisation of OS is often hindered by sensitivity challenges posed by their trace amount in typical biological matrices (*e.g.*, plasma, tissue, cells, etc.) [32], as well as by the presence of numerous isomeric species that cannot be reliably differentiated using only high-resolution mass spectrometry (HRMS). These issues were recently addressed using a newly developed [17] liquid chromatography (LC)-MS method that does not require any preliminary chemical derivatisation to enhance OS detection. The reversed-phase (RP)LC selectivity offered by the cyanopropyl (ES-CN) and pentafluorophenyl (F5) stationary phases was combined to ensure the reliability of the qualitative and quantitative results. These RPLC methods were first optimized for the separation of 10 OS (25-HC, 24(S)-HC, 26(R/S)-HC, CT, 7α-HC, 7β-HC, 7-KC, 5α,6α-EC, and 5β,6β-EC), and subsequently were found to be effective for the separation of 4 additional OS, namely, 4β-hydroxycholesterol (4β-HC), 22(R)-hydroxycholesterol (22(R)-HC), 22(S)-hydroxycholesterol, and 7α,25-dihydroxycholesterol (7α,25-HC). This finding underscores the versatility and robustness of the RPLC methods, which outperform existing approaches for the separation of native OS, many of which fail to achieve unambiguous MS identification due to overlapping ionization pathways [17].

Overall, a clear trend emerged in the quantitative profiles of ring oxysterols (OS). Under normoxic conditions, PANC-1 cells exhibited statistically significant higher levels of CT, 7α-HC, 7β-HC, and 7-KC compared with HPNE cells. In contrast, under hypoxic conditions, ring OS levels were more comparable between the two cell types. Notably, the abundance of the 26(R/S)-HC epimers was particularly sensitive to oxygen availability during cell growth. The high sensitivity and selectivity of the LC–MS method enabled, for the first time, the characterisation of the qualitative OS profiles of the corresponding extracellular vesicles (EVs). These phospholipid bilayer-enclosed nanoparticles are released by cells that mediate clinically relevant intercellular

communication [33] and are key effectors of tumour progression and microenvironmental remodelling [34]. In EVs, 25-HC and epoxycholesterol isomers contributed more prominently to the OS profile than in the parent cells, suggesting a selective enrichment of specific OS species during EV formation.

## 2. Materials and methods

### 2.1. Chemicals

Potassium hydroxide (≥99.95% purity), phosphate buffer saline tablets, HPLC grade (≥95% purity) dichloromethane, LC-MS grade acetonitrile, isopropanol, methanol, formic acid and water were purchased from Merck (Milan, Italy). The list of analytical standards obtained from Cayman Chemicals (Ann Arbour, USA) and Avanti Polar (Alabaster, USA), along with their structures and mass spectral data, is reported in Supporting Information (Table S1 and Fig. S1).

### 2.2. LC-MS instrumentation and operating conditions

LC-MS analyses were performed using a platform consisting of an Ultimate 3000 HPLC quaternary chromatographic system and a Q-Exactive high-resolution quadrupole-Orbitrap mass spectrometer (Thermo Fisher Scientific, Waltham, USA). The chromatographic column eluent was transferred into the heated electrospray ionization (HESI) interface (Thermo Fisher, West Palm Beach, CA, USA) mounted on the mass spectrometer. RPLC separations were performed using two different HPLC columns, supplied by Supelco (Bellefonte, USA): an Ascentis Express HPLC column 90 Å ES-CN (cyanopropyl), and an Ascentis Express HPLC column 90 Å F5 (pentafluorophenyl). The columns shared identical length (15 cm), internal diameter (2.1 mm), and dimensions of the packing spherically porous (core-shell) particles (2.7 μm).

Separation conditions on both the ES-CN and F5 columns were previously optimized with the assistance of the DryLab® software [17]. Here, some slight modifications were introduced for improved column washing and reconditioning.

For ES-CN: *Eluent composition*: water (solvent A) and 18% v/v mixture of methanol in acetonitrile (solvent B) both spiked with formic acid (0.1% v/v), *Multilinear gradient structure*: 0 - 50 min) linear increase of B from 40% to 62.5%; 50 - 55 min) linear increase of B from 62.5% to 100%; 55 - 60 min) isocratic at 100% of B; 60 – 65 min) linear decrease of B from 100% to 40%; 65 - 75 min) isocratic at 40% of B, *Flow-rate*: 0.25 mL/min, *Column temperature*: 50 °C.

For F5: *Eluent composition*: water (solvent A) and a 47% v/v mixture of methanol in acetonitrile (solvent B) both spiked with formic acid (0.1% v/v), *Multilinear gradient structure*: 0 - 35 min) linear increase of B from 55% to 72.5%; 35 - 40 min) linear increase of B from 72.5% to 100%; 40 - 50 min) isocratic at 100% of B; 50 – 55 min) linear decrease of B from 100% to 55%; 55 - 65 min) isocratic at 55% of B, *Flow-rate*: 0.25 mL/min, *Column temperature*: 25 °C.

In the case of F5 stationary phase, column temperature was not included among the parameters considered for method optimization with DryLab®. Indeed, high temperatures (>25 °C), combined with the presence of methanol in the mobile phase, were proven to introduce heavy retention artifacts specifically involving ring-oxysterols such as 7-hydroxycholesterol epimers and 5,6-epoxycholesterol isomers. On the other hand, the ES-CN stationary phase was proven to be less affected by such effects and the use of higher temperatures has been explored to reach the best possible quality compromise for the separation of the target analytes [17].

The parameters of the HESI interface and the ion optics of the Q-Exactive mass spectrometer were set as follows: sheath gas flow rate: 35 a.u.; auxiliary gas flow rate: 15 a.u.; spray voltage: 3.5 kV; capillary temperature: 320 °C; S-lens RF level: 50; auxiliary gas temperature: 40 °C. The Q-Exactive mass spectrometer was operated at its maximum resolving power (140000 at *m/z* 200) for *full scan* experiments. *Full-scan* Fourier Transform mass spectra (FTMS) were acquired in a 200-500 *m/z* interval setting the Automatic Gain Control (AGC) level at $1 \times 10^6$, and the maximum injection time at 500 ms. The mass spectrometer was calibrated on alternate days by infusing, at a 5 μL/min flow rate, calibration solutions provided by the instrument manufacturer for both negative and positive polarity acquisitions. As a result, mass accuracy was always lower than 5 ppm.

### 2.3. Culture conditions for HPNE and PANC-1 cells

HPNE (immortalized human pancreatic ductal epithelial cells, representing non-tumourigenic pancreatic cells) and PANC-1 (human pancreatic ductal adenocarcinoma cells) were obtained from ATCC (Manassas, VA, USA) and cultured in T75 flasks at 37 °C in a humidified atmosphere with 5% $CO_2$. PANC-1 cells were cultured in RPMI 1640 medium (Gibco, Thermo Fisher Scientific; cat. no. 21875) supplemented with 10% fetal bovine serum (FBS; Gibco, Thermo Fisher Scientific; cat. no. A5256701). HPNE cells were grown in low-glucose Dulbecco's Modified Eagle Medium (DMEM; Gibco, Thermo Fisher Scientific; cat. no. 31885023) supplemented with 5% FBS and 10 ng/mL human recombinant epidermal growth factor (EGF; Gibco, Thermo Fisher Scientific; cat. no. AF-100-15-500μg). Both media were further supplemented with 1% penicillin-streptomycin (Gibco, Thermo Fisher Scientific; cat. no. 15070-063). For hypoxic conditions, once cells reached approximately 70–75% confluency, they were placed in a hypoxic glove box (O2 Control InVitro, CoyLabs, Grass Lake, MI) and cultured at 37 °C under 1% $O_2$ for 48 h. After treatment, the cells were washed with PBS (Gibco, Thermo Fisher Scientific, cat. no. 10010023), detached using 0.25% trypsin–EDTA (Gibco, Thermo Fisher Scientific, cat. no. 25200056) and centrifuged at 250×*g*. Pellets were then washed again with PBS and recentrifuged.

### 2.4. Extracellular vesicles isolation and characterization

Cells were cultured in T175 flasks and, upon reaching ~80% confluency, incubated in FBS-free medium for 48 h. The conditioned medium was collected and sequentially centrifuged at 250×*g* for 5 min and 2000×*g* for 30 min to remove cells and debris. The clarified supernatant was concentrated to ~1 mL using a 100 kDa MWCO filter (Thermo Fisher Scientific, cat. no. 88532). Total Exosome Isolation Reagent (Thermo Fisher Scientific, cat. no. 4478359) was added at a 1:2 ratio (reagent/medium), mixed, and incubated overnight at 4 °C. The following day, the samples were centrifuged at 10,000×*g* for 1 h, the supernatant discarded, and the resulting EV pellet collected [35]. Consistently with our previous works [35,36], the size distribution and concentration of isolated EVs were determined by nanoparticle tracking analysis (NTA) using a NanoSight LM10 (Malvern Instruments, UK) equipped with a 405 nm laser and NTA 3.2 software. Moreover, the EVs profile was characterized by Western blot analysis as detailed in Supplementary information.

### 2.5. Oxysterol extraction from cell pellets and extracellular vesicles

The extraction workflow was adapted from the protocol proposed by McDonald et al. [37], with small modifications aimed at minimising sample treatment. Although solid-phase extraction (SPE) was proposed [37] to remove endogenous cholesterol and minimise the risk of its chemical oxidation during the extraction process, the SPE step was omitted in the present study to enable direct semi-quantitative determination of endogenous cholesterol. To this aim, samples were initially spiked with a known amount of d7-cholesterol, which additionally allowed monitoring of any potential oxidation occurring during the extraction procedure.

The extraction protocol can be summarized as follows: the EV or cell pellet was resuspended in 1 mL of isopropanol. The dispersion was

spiked with 100 μL of a 1 mg/mL solution of d7-cholesterol and 50 μL of a solution containing d6-25-HC and d7-5α,6α-EC, both at concentrations of 10 μg/mL. The sample was subjected to ultrasound homogenization using an UP200St probe-type ultrasonic homogeniser (Hielscher Ultrasonic, Teltow, Germany) operating at 40% amplitude for 5 s. The homogenate was quantitatively transferred into 15 mL glass centrifuge tubes before the addition of 3 mL of a 50% v/v solution of $CH_2Cl_2$/$CH_3OH$. The overall mixture was incubated at 30 °C for 10 min under moderate agitation (700 rpm) by an orbital thermoshaker (IKA, Staufen, Germany). The liquid phase was separated from the remaining pellet residue by centrifugation (1970×*g*, 10 min). Additional 3 mL of the $CH_2Cl_2$/$CH_3OH$ mixture was added to the solid residue, and the mixture was re-incubated at 30 °C for 10 min at the same agitation rate (700 rpm). The liquid phase was recovered by centrifugation, and the two supernatants were combined. Thereafter, 300 μL of a 10 mol/L solution of potassium hydroxide (KOH) was added, and the mixture was incubated at 40 °C for 90 min under moderate agitation (700 rpm) to promote the hydrolysis of the ester bonds of acylated OS. The organic phase was washed with 3 mL of 50 mmol/L phosphate-buffered aqueous solution to remove excess KOH. Once a stable phase separation was achieved after centrifugation (1970×*g* for 10 min), the organic phase was withdrawn and transferred into 10 mL glass tubes. The remaining aqueous medium was washed with 3 mL of $CH_2Cl_2$. The $CH_2Cl_2$-rich phase was recovered after centrifugation (1970×*g* for 10 min) and combined with the previously collected $CH_2Cl_2$/$CH_3OH$ extract. The overall mixture was subjected to solvent evaporation using a SpeedVac concentrator (Thermo Fisher Scientific, Waltham, USA). The dried residue was reconstituted in 200 μL of $CH_2Cl_2$/$CH_3OH$ and diluted by a 1:1 factor in $CH_3CN$ before RPLC-HESI-FTMS analysis. In the case of EVs, the three extracts obtained from each EV type were pooled, dried, and resuspended in 200 μL of $CH_2Cl_2$/$CH_3OH$ to increase the quality of the LC-MS signal, prior to the 1:1 dilution with $CH_3CN$ (*vide infra*).

### 2.6. Evaluation of cellular oxidative stress

CellROX Green Reagent (Thermo Fisher Scientific, cat. no. C10444) was added to the culture medium at a final concentration of 5 μM and incubated for 30 min according to the manufacturer's instructions. For each condition, the samples were prepared alongside negative (medium without CellROX Green Reagent) and positive controls (medium containing CellROX Green Reagent and hydrogen peroxide at a final concentration of 500 μM).

## 3. Results and discussion

### 3.1. LC-MS-based characterisation of oxysterols in healthy and pancreatic tumour cells

The separation of cholesterol and the 14 targeted OS analytes was accomplished within 55 min using RPLC methods employing

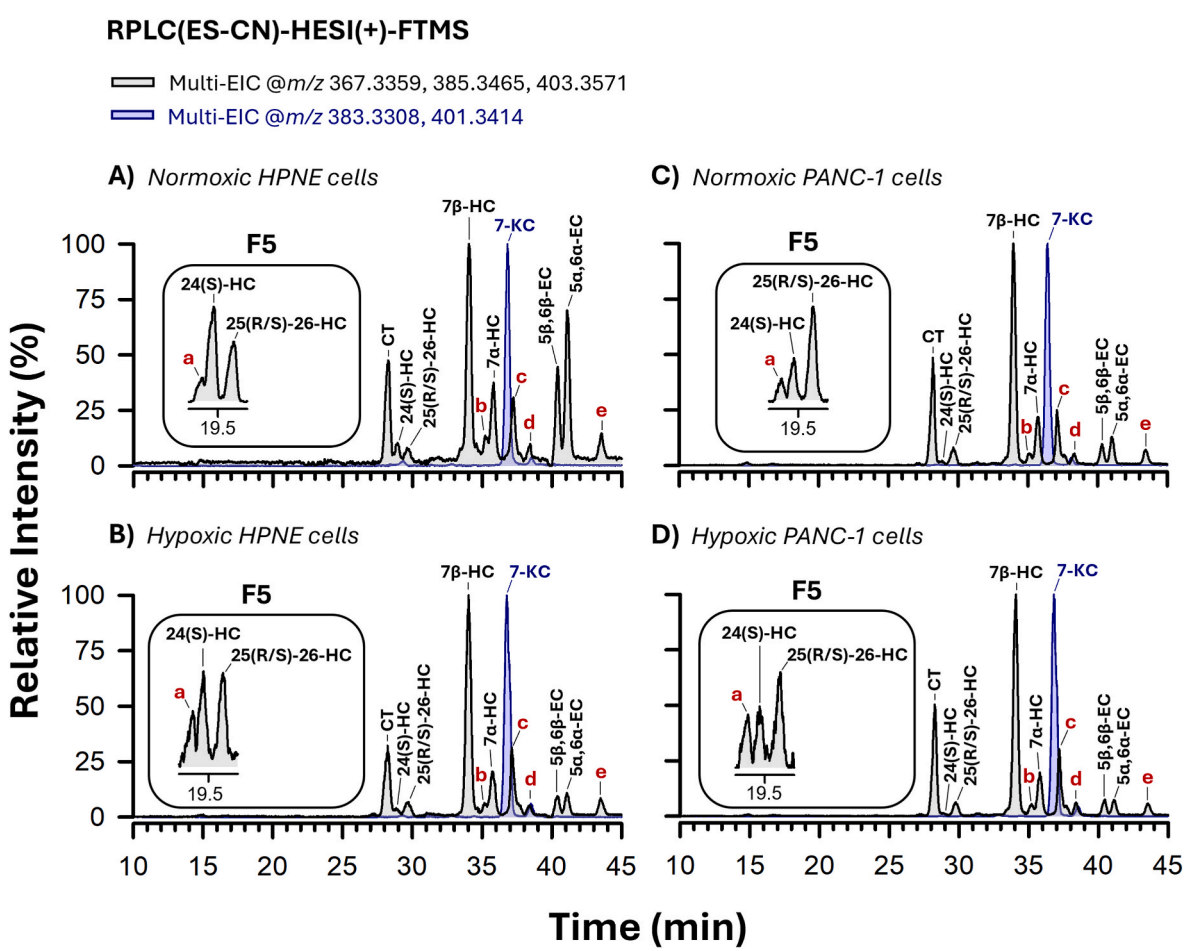


**Fig. 1.** RPLC–HESI(+)-FTMS multiple extracted-ion current (multi-EIC) chromatograms obtained for HPNE (panels A and B) and PANC-1 (panels C and D) cells cultured under normoxic and hypoxic conditions. Separations were performed using a cyanopropyl stationary phase (ES-CN). The presence of 7-ketocholesterol (7-KC) and 7α,25-dihydroxycholesterol (7α,25-HC) was evaluated by monitoring their characteristic ionization pathways (*m/z* 383.3308 and 401.3414), which differ from those used for the remaining oxysterol standards (*m/z* 367.3359, 385.3465, and 403.3571; see Table S1). Insets show expanded chromatographic regions highlighting the separation of side-chain oxysterols obtained with the pentafluorophenyl (F5) column. Unidentified or ambiguous peaks are labelled with lowercase letters (a–e) according to elution order. Oxysterol nomenclature follows the conventions defined in the list of abbreviations.

cyanopropyl (ES-CN) and pentafluorophenyl (F5) stationary phases (Fig. S2). In both chromatographic approaches, the selectivity was insufficient to resolve the peaks corresponding to 25(R)-26-HC and 25(S)-26-HC epimers. Of the 14 targeted OS, 24(S)-HC, 25(R/S)-26-HC, CT, 7β-HC, 7α-HC, 7-KC, 5β,6β-EC, and 5α,6α-EC were confidently detected in normoxic and hypoxic HPNE and PANC-1 cell lines based on retention time alignment (Fig. 1).

Upon application of the ES–CN–based RPLC method, the accuracy of 24(S)-HC peak integration was hampered by the lack of baseline separation between CT and 24(S)-HC (Fig. S2A), together with the pronounced dominance of the CT signal. On the other hand, no peak overlap was observed between CT and 24(S)-HC when separation was performed using F5 as the stationary phase (Fig. S2B). Therefore, the quantification of 24(S)-HC, as well as 25(R/S)-26-HC, was based on the F5-based LC-MS method.

Although the use of the F5 column offers a shorter analysis time compared to the ES-CN column, it is known to induce retention artifacts that specifically affect side-chain OS, including 7-HC epimers and 5,6-EC isomers [17]. No peak alterations were observed when ring-OS were separated using the ES–CN–based method [17]. Therefore, the latter approach was used for the quantification of all ring-OS species, namely CT, 7β-HC, 7α-HC, 7-KC, 5β,6β-EC, and 5α,6α-EC.

As illustrated in the insets of Figs. 1 and 24(S)-HC partially co-eluted with an early-eluting, unidentified compound (denoted as peak "**a**") when chromatographic separation was performed on the F5 column. Although the retention time of this peak matched that of the 25-HC analytical standard under identical conditions, its identity could not be confirmed, as no corresponding 25-HC signal was detected when the separation was carried out on the ES-CN column. Conversely, peak "**e**" observed on the ES-CN column (Fig. 1) exhibited a retention time consistent with that expected for 4β-HC. However, this assignment could not be corroborated on the F5 column, where no signal attributable to 4β-HC was observed. To ensure robustness and consistency of the results, OS quantification was restricted to species that were unambiguously identified based on matching retention times on both chromatographic columns. When this criterion was satisfied, analyte identities were further validated by comparing their in-source fragmentation patterns in cellular samples with those of the corresponding analytical standards (Table S2). When operating in positive ion mode, the electrospray ionization of OS, co-adjuvated by the presence of formic acid, predominantly results in the formation of $[M+H]^+$ ion adducts. The protonation is likely to involve either the oxygenated moieties (*i.e.*, hydroxyl and keto groups) or the double bond (if present) inherited from the cholesterol structure. In the latter case, a carbocation is generated. The carbocation can be further stabilized in its allylic or bis-allylic form via the elimination of one or two water molecules, involving one or two hydroxyl groups suitably positioned relative to the positive charge. Hydroxyl groups located on the sterol side chain can be also lost as water molecules through charge-remote fragmentation in case highly substituted alkenes are formed. These mechanistic hypotheses have been thoroughly described in our recent publication [17] and can be invoked to justify the propensity of certain OS to undergo extensive in-source fragmentation. The latter results in the formation of $[M + H-nH_2O]^+$ ions, where the $n$ value depends on the number of hydroxyl groups that can be involved in the elimination of neutral water molecules. As a result, distinctive in-source fragmentation patterns can be observed for the majority of the 14 targeted oxysterols. For each compound, information on both the ion type and the intensity distribution across the corresponding ion channels is provided in Table S1. Careful evaluation of these fragmentation patterns was essential to exclude potential interferences and to guarantee accurate quantification of the targeted OS species.

As shown in Fig. 1, signals corresponding to CT, the 7-HC epimers, and the 5,6-epoxycholesterol isomers were markedly more intense than those of 24(S)-HC and 25(R/S)-26-HC. These ring oxysterols, together with 7-KC, could in principle originate from oxidation of endogenous cholesterol during sample preparation. However, this possibility was excluded based on the results reported in Fig. S3, which show that no oxidation products were detected from d7-cholesterol spiked into the samples prior to extraction. The amount of d7-cholesterol added was adjusted to closely match the endogenous cholesterol content. Further details on oxysterol quantification are provided in Section S1. Cholesterol was quantified using a semi-quantitative approach, whereby endogenous cholesterol levels were calculated by multiplying the peak area ratio of cholesterol to d7-cholesterol by the known amount of d7-cholesterol added to each sample (100 μg). For all target analytes, concentrations were normalised to cell number and expressed per million cells.

### 3.2. Quantitative characterization of oxysterols in healthy and tumour pancreatic cells

Quantitative profiling of OS revealed marked differences between healthy pancreatic cells and PDAC cells, with these alterations being strongly modulated by oxygen availability during cell culture. In both HPNE and PANC-1 cells, the abundance of several OS species showed pronounced sensitivity to oxygen levels. These trends are summarized in the bar charts shown in Fig. 2, which report the levels of the eight detected OS as a function of cell type under normoxic and hypoxic conditions. The figure also includes a graphical representation of the estimated 95% confidence intervals (CIs), calculated from biological replicates for each cell line; the corresponding CI widths are reported in Table S4.

Across both normoxic and hypoxic conditions, the average estimated amounts of CT, 7α-HC, 7β-HC, and 7-KC were consistently higher in PANC-1 cells than in healthy HPNE cells. This behaviour may be attributed to enhanced oxidative stress in tumour cells. As shown in Fig. S4, a two-tailed *t*-test revealed significantly higher ROS levels in PANC-1 cells compared with HPNE cells under both growth conditions. In addition, reduced oxygen bioavailability promoted the accumulation of CT, 7α-HC, 7β-HC, and 7-KC in both cell lines. Consequently, the differences observed between healthy and tumour cells under normoxic conditions were further amplified when normoxic HPNE cells were compared with hypoxic PANC-1 cells. Moreover, cholesterol levels were slightly but significantly increased when both cell types were cultured under hypoxic conditions. The statistical robustness of these observations was evaluated using appropriate tests for comparison of means. The homogeneity of variance (homoscedasticity) was assessed using Bartlett's test, as a fundamental prerequisite for choosing the most appropriate statistical approach for comparison of means. Depending on the outcome, either the analysis of variance (ANOVA) as a parametric test or the Kruskal–Wallis test (*i.e.*, its non-parametric alternative) was applied. For ANOVA, Tukey's test was employed as a *post hoc* test, while Dunn's test was used as the corresponding *post hoc* analysis in the case of heteroscedasticity. All tests were conducted at a 95% confidence level.

Significant differences between group means were detected by the ANOVA test for 7α-HC, 7-KC, and 24(S)-HC. The Tukey's post hoc test confirmed significantly lower 7α-HC levels in normoxic HPNE cells compared with normoxic PANC-1 cells. Hypoxia induced a significant increase in 7α-HC levels in HPNE cells, which became comparable to those observed in normoxic PANC-1 cells. By contrast, 7α-HC levels in hypoxic PANC-1 cells were significantly higher than in all other cell types and conditions. A similar trend was observed for 7-KC; however, no statistically significant differences in 7-KC levels were detected among normoxic HPNE, normoxic PANC-1, and hypoxic HPNE cells.

Significant differences between group means were detected by the Kruskal–Wallis test for both CT and 7β-HC. In both cases, Dunn's post hoc test revealed a statistically significant variation only between normoxic HPNE and hypoxic PANC-1 cells. It should be noted that, even when within-group variability is low and group separation is evident, Dunn's test may lack sufficient statistical power to detect significant differences, particularly when rank differences are small or sample sizes

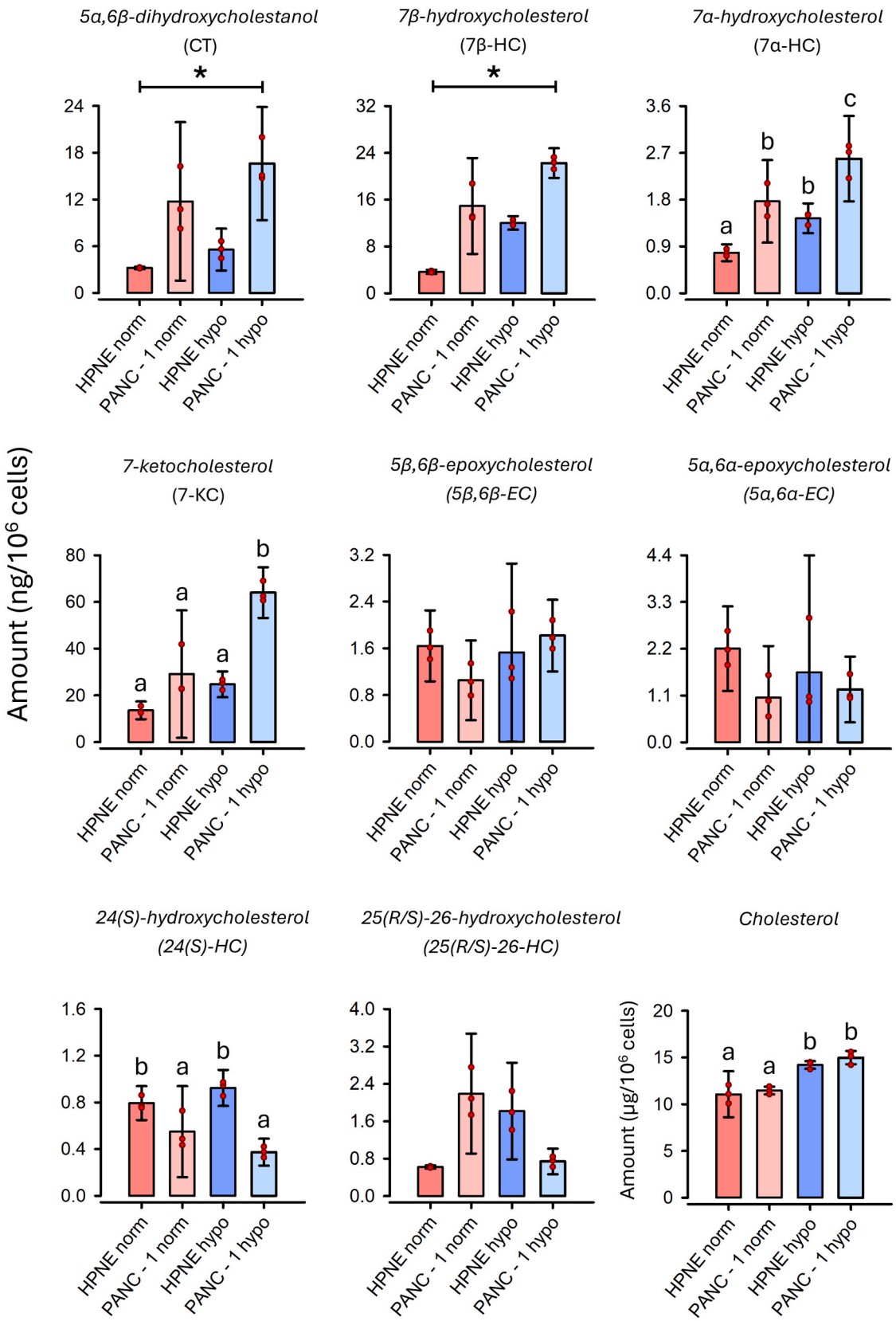


**Fig. 2.** Amounts of cholesterol and eight oxysterols measured in HPNE and PANC-1 cells cultured under normoxic (norm) and hypoxic (hypo) conditions. Bars represent mean values (n = 3), with individual replicates shown as overlaid points. Error bars indicate 95% confidence intervals. Statistical significance was assessed using one-way ANOVA followed by Tukey's post hoc test when homoscedasticity was confirmed by the Bartlett test. Groups that differ significantly ($p < 0.05$) are denoted by different letters. The Kruskal–Wallis test was used as the non-parametric alternative to ANOVA in cases of heteroscedasticity. In such cases, pairwise comparisons were performed using Dunn's post hoc test. Statistically significant differences ($0.01 \leq p < 0.05$) are indicated by asterisk (*)-labelled connection lines. Bonferroni-adjusted p-values were considered for multiple comparisons.

are limited. Consistently, inspection of the overlap between the calculated CIs for CT and 7β-HC across all sample types revealed a scenario that is globally coherent with that described for 7α-HC and 7-KC.

Similarly to CT, 7α-HC, 7β-HC, and 7-KC, both 5α,6α-EC and 5β,6β-EC can be generated through ROS-mediated oxidation of cholesterol. Nevertheless, ANOVA did not reveal significant differences between group means for these epoxycholesterol isomers across all cell types and conditions. A distinct behaviour was observed for side-chain OS. According to Tukey's test, 24(S)-HC levels depended primarily on cell type rather than oxygen availability, with significantly higher amounts detected in HPNE cells compared with PANC-1 cells under both normoxic and hypoxic conditions. Conversely, no statistically significant differences were identified by the Kruskal–Wallis test for 26(R/S)-HC. However, based on average values and evaluation of CI overlap, the abundance of this oxysterol appeared to be strongly modulated by oxygen availability, exhibiting opposite trends in the two cell lines. Specifically, hypoxic conditions led to increased 26(R/S)-HC levels in HPNE cells, whereas a decrease was observed in PANC-1 cells. As a result, comparable levels of 26(R/S)-HC were detected in normoxic HPNE and hypoxic PANC-1 cells.

Beyond absolute OS amounts, discrimination between healthy and PDAC cells can also be achieved by evaluating OS profile data, as shown in Fig. S5. The contribution of each OS species to the overall profile was calculated as the percentage ratio (%RA) between its amount and the sum of all detected OS. Equivalent information can be derived from extracted-ion current peak areas, allowing qualitative profile differences to be inferred directly from chromatographic traces. However, the application of multivariate statistical approaches provides a more robust and intuitive evaluation of profile data. Accordingly, Fig. 3 reports the score and loading plots obtained from principal component analysis (PCA) of the OS profiles. The scores of normoxic HPNE and PANC-1 cells are clearly separated along PC1. This separation is mainly driven by differences in the relative abundance of specific *ring*-OS generated by ROS-mediated cholesterol oxidation. 7β-HC and CT were markedly increased in PANC-1 cells, whereas the opposite trend was observed for 5α,6α-EC and 5β,6β-EC, resulting in a higher relative abundance of epoxycholesterol isomers in HPNE cells. This behaviour is also evident from the comparison of the chromatographic profiles shown in plots A and C of Fig. 1. The loading plots in Fig. 3 further highlight the contribution of 7-KC to the separation along PC1. Although 7-KC levels increased in PANC-1 cells, this increase was less pronounced than that observed for 7β-HC and CT, leading to a slightly lower %RA compared with normoxic HPNE cells. Consistently, the difference in %RA for 7-KC between normoxic HPNE and PANC-1 cells was not statistically significant (Fig. S5).

In addition to intrinsic differences between healthy and tumour cells, oxygen deprivation induced opposite modifications of the OS profiles in the two cell lines. Hypoxic HPNE scores shifted toward normoxic PANC-1 cells along PC1, reflecting hypoxia-induced accumulation of *ring*-OS such as CT and 7-HC epimers, while epoxycholesterol levels remained comparable to normoxic conditions. In contrast, hypoxic PANC-1 cells exhibited a less pronounced increase in these species, resulting in a shift toward normoxic HPNE cells along PC1. Notably, 7-KC levels were consistently elevated in hypoxic PANC-1 cells, yielding a higher %RA and enabling separation from normoxic HPNE cells along PC2 (Fig. 3A). Conversely, hypoxic HPNE and normoxic PANC-1 cells were better separated along PC3 due to the higher %RA of CT in the latter (Fig. 3C). Overall, PCA indicates that hypoxia induces a convergent remodelling of oxysterol profiles in healthy and PDAC cells, while preserving cell-type–specific signatures driven by differential regulation of ring-oxidized species.

### 3.3. Qualitative characterisation of oxysterols in EV from healthy and tumour pancreatic cells

Extracellular vesicles (EVs) are membrane-bound particles released by cells into the extracellular environment and act as carriers of bioactive molecules, including proteins, lipids, and nucleic acids, thereby playing a key role in intercellular communication [38]. Owing to these properties, EVs have been extensively investigated as a potential source

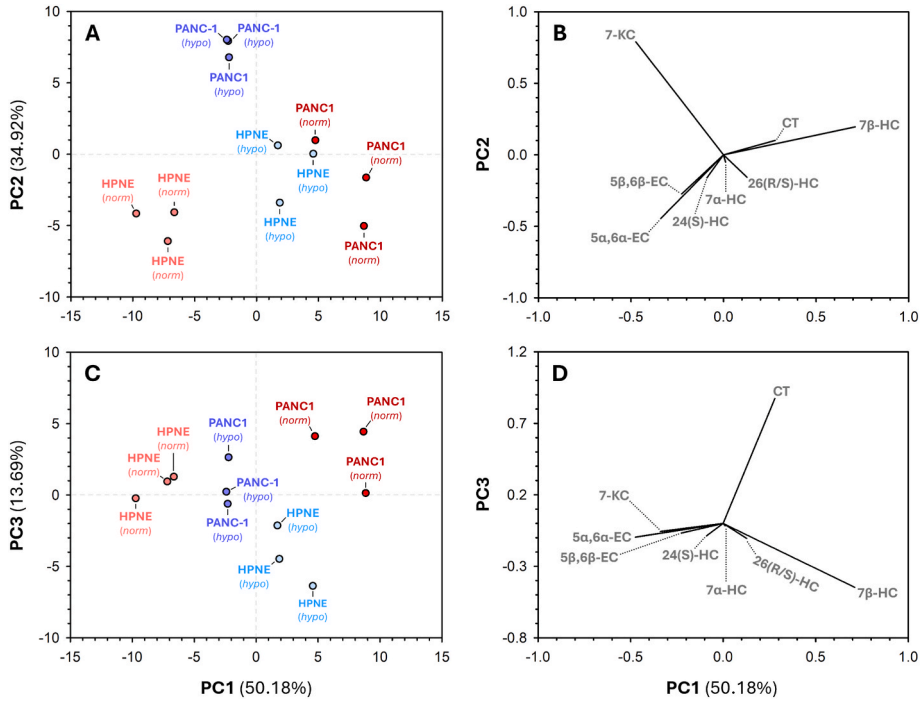


**Fig. 3.** Principal component analysis (PCA) of oxysterol profiles from HPNE and PANC-1 cells cultured under normoxic (norm) and hypoxic (hypo) conditions. Data were mean centered without autoscaling. Two-dimensional score and loading plots are shown, with PC2 versus PC1 (panels A and B) and PC3 versus PC1 (panels C and D). The percentage of variance explained by each principal component is reported along the corresponding axes. In the score plots, biological replicates are indicated by the same color.

of circulating biomarkers for the early diagnosis of PC [38]. On this basis, the present study extended the LC-MS characterisation of OS to EVs produced by HPNE and PANC-1 cells cultured under normoxic and hypoxic conditions. Triplicate EV samples were obtained using the isolation protocol described in the Materials and Methods section. EV size distribution and identity were assessed by nano tracking analysis (NTA) and Western blot (WB) analysis (Fig. S6), both of which confirmed the successful isolation of EVs. In accordance with current guidelines for extracellular vesicles [39], WB analysis demonstrated positivity for established EV markers, including transmembrane proteins (CD63 and CD9) and cytosolic proteins (ALIX and FLOT1), as well as negativity for markers of other intracellular compartments (CANX, endoplasmic reticulum/Golgi apparatus marker). The results of these analyses are summarized in Fig. S6, while technical details regarding NTA and WB experiments are provided in Sections S2 and S3, respectively. To confirm uniform sample loading in WB analysis, the original stain-free total protein profiles are included in Fig. S7.

OS were detected in trace amounts in the cell samples, and even lower abundances were expected in the corresponding EV samples. Accordingly, OS signals were barely distinguishable in the EIC chromatograms obtained from individual EV replicates. To increase OS detectability, EV extracts from replicate samples were pooled, which precluded statistical analysis of quantitative data. Consequently, the present investigation was limited to the qualitative profiling of OS in EV samples, with primary emphasis on accurate compound identification. Nevertheless, meaningful information could be obtained by comparing the EIC traces of the EV samples (Fig. 4) with those of the corresponding cell samples (Fig. 2).

Except for 25-HC, no OS other than those already detected in the parent cell samples were confidently identified in EVs based on retention time and mass spectrometric information derived from analytical standards. The presence of 25-HC was confirmed in EVs from all conditions except those produced by hypoxic PANC-1 cells, in which the signal was barely detectable in the EIC traces (Fig. 4D). Notably, all EV samples exhibited highly similar EIC profiles, which differed from those of the corresponding cell samples mainly due to the predominance of 5β,6β-epoxycholesterol (5β,6β-EC). In addition, the intensity of the 7α-hydroxycholesterol (7α-HC) peak was comparable to that of its 7β epimer in EV samples, whereas a lower 7α-HC/7β-HC intensity ratio was consistently observed in all cell samples. Regarding side-chain OS, 24 (S)-hydroxycholesterol was not detected in EVs produced by either HPNE or PANC-1 cells cultured under hypoxic conditions. In contrast, 26 (R/S)-hydroxycholesterol was detected in EVs derived from all investigated cell types and oxygenation conditions.

Overall, EVs displayed a conserved yet distinct oxysterol fingerprint compared with their parent cells, characterized by selective enrichment of specific ring-oxidized species and limited representation of side-chain oxysterols, highlighting a regulated sorting mechanism rather than passive lipid transfer. These findings suggest that future and in-depth quantitative evaluation of EV-borne oxysterols, particularly under varying oxygenation conditions, may provide functionally relevant signatures and warrant further investigation in clinically accessible biofluids to assess their potential as biomarkers and mediators of pancreatic cancer progression.

## 4. Conclusions

This study demonstrates that oxysterol profiles in pancreatic cells are strongly influenced by both tumour phenotype and oxygen availability. PANC-1 tumour cells exhibited a consistent enrichment of ring-oxidized oxysterols regardless of oxygenation conditions, supporting the presence of a disease-associated chemical signature potentially linked to oxidative stress and/or metabolic reprogramming. Hypoxia further amplified the accumulation of these species, highlighting oxygen limitation as a

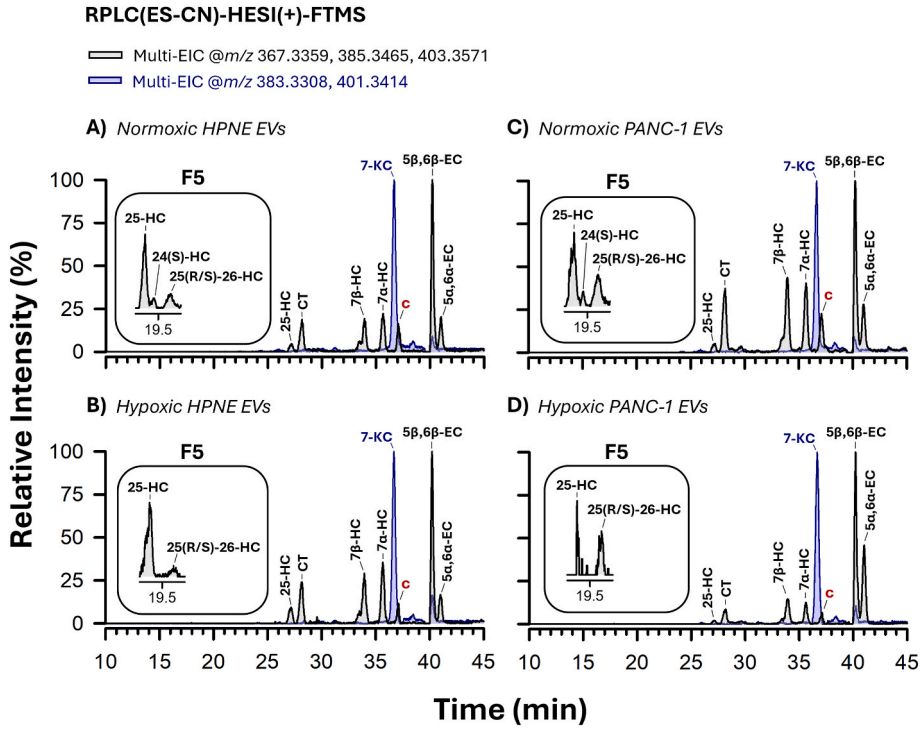


**Fig. 4.** RPLC–HESI(+)-FTMS multi-EICs chromatograms obtained for extracellular vesicle (EV) samples derived from HPNE (panels A and B) and PANC-1 (panels C and D) cells cultured under normoxic and hypoxic conditions. Separations were performed using a cyanopropyl stationary phase (ES-CN). The presence of 7-ketocholesterol (7-KC) and 7α,25-dihydroxycholesterol (7α,25-HC) was evaluated by monitoring their characteristic ionization pathways (*m/z* 383.3308 and 401.3414), which differ from those used for the remaining oxysterol standards (*m/z* 367.3359, 385.3465, and 403.3571; see Table S1). Insets show expanded chromatographic regions highlighting the elution of side-chain oxysterols obtained using the pentafluorophenyl (F5) column. Unidentified peaks detected in the corresponding cell samples are labelled using the same lowercase letter notation as in Fig. 1.

key modulator of oxysterol homeostasis. Side-chain oxysterols displayed divergent behaviors, with 24(S)-hydroxycholesterol primarily associated with cell type and 26(R/S)-hydroxycholesterol highly sensitive to hypoxic conditions in a cell-specific manner. Extracellular vesicles mirrored cellular oxysterol content while displaying a distinct enrichment of 25-hydroxycholesterol and 5β,6β-epoxycholesterol. Together, these findings support the relevance of oxysterols as dynamic metabolic players in pancreatic cancer and demonstrate the suitability of the proposed LC–MS strategy for future investigations in clinically relevant biological matrices, including tissues and biofluids, as well as for deepening the understanding of the possible regulatory role that oxysterols may play in the onset and development of pancreatic cancer. Future in vivo studies will be essential to validate these observations within the complex tumour microenvironment and to assess the translational potential of oxysterol signatures as biomarkers or therapeutic targets.

## Funding source

This work was supported by the project "LIpidome of extracellular VEscicles in hypoxic pancreatic cancer" acronimo "LIVE" CUP - H93C24000620006, Bando a cascata emanato dallo Spoke 6 del Tuscany Health Ecosystem a valere sulle risorse del PNRR, M4C2 - Investimento 1.5 – creazione e rafforzamento di "Ecosistemi dell'innovazione per la sostenibilità", financed by the European Union – NEXT GENERATION EU; and the project Life Science Hub Regione Puglia (LSH-Puglia, T4-AN-01H93C22000560003).

## CRediT authorship contribution statement

**Vito Nettis:** Conceptualization, Data curation, Formal analysis, Investigation, Methodology, Visualization, Writing – original draft. **Andrea Castellaneta:** Conceptualization, Data curation, Formal analysis, Investigation, Methodology, Validation, Visualization, Writing – original draft. **Noa Ndimurwanko:** Data curation, Formal analysis, Investigation, Methodology, Visualization, Writing – original draft. **Francesco Greco:** Data curation, Formal analysis, Investigation. **Valentina Casieri:** Data curation, Formal analysis, Investigation, Visualization. **Vincenzo Lionetti:** Data curation, Formal analysis, Investigation, Visualization. **Elisa Giovannetti:** Resources, Supervision, Visualization, Writing – review & editing. **Liam A. McDonnell:** Funding acquisition, Project administration, Supervision, Validation, Writing – review & editing. **Tommaso R.I. Cataldi:** Resources, Supervision, Validation, Writing – review & editing. **Cosima D. Calvano:** Funding acquisition, Project administration, Resources, Supervision, Validation, Writing – review & editing.

## Declaration of competing interest

The authors declare that they have no known competing financial interests or personal relationships that could have appeared to influence the work reported in this paper.

## Acknowledgements

The authors acknowledge Dr. Imre Molnár and the team at the Molnár-Institute for their valuable scientific support in the development and application of the chromatographic strategies adopted in this work.

## Appendix A. Supplementary data

Supplementary data to this article can be found online at https://doi.org/10.1016/j.talanta.2026.129885.

## Data availability

Data will be made available on request.

## References

[1] F. Bray, M. Laversanne, H. Sung, J. Ferlay, R.L. Siegel, I. Soerjomataram, A. Jemal, Global cancer statistics 2022: GLOBOCAN estimates of incidence and mortality worldwide for 36 cancers in 185 countries, CA Cancer J. Clin. 74 (2024) 229–263, https://doi.org/10.3322/caac.21834.

[2] J.M. Kocarnik, K. Compton, D, et al., Cancer incidence, mortality, years of life lost, years lived with disability, and disability-adjusted life years for 29 cancer groups from 2010 to 2019 A systematic analysis for the global burden of disease study 2019, JAMA Oncol. 8 (2022) 420–444, https://doi.org/10.1001/jamaoncol.2021.6987.

[3] A. Carrato, A. Falcone, M. Ducreux, J.W. Valle, A. Parnaby, K. Djazouli, K. Alnwick-Allu, A. Hutchings, C. Palaska, I. Parthenaki, A systematic review of the burden of pancreatic cancer in Europe: real-world impact on survival, quality of life and costs, J. Gastrointest. Cancer 46 (2015) 201–211, https://doi.org/10.1007/s12029-015-9724-1.

[4] R.L. Siegel, K.D. Miller, A. Jemal, Cancer statistics, CA Cancer J. Clin. 70 (2020) 7–30, https://doi.org/10.3322/caac.21590, 2020.

[5] C. Neuzillet, S. Gaujoux, N. Williet, J.-B. Bachet, L. Bauguion, L. Colson Durand, T. Conroy, L. Dahan, M. Gilabert, F. Huguet, L. Marthey, J. Meilleroux, L. de Mestier, B. Napoléon, F. Portales, A. Sa Cunha, L. Schwarz, J. Taieb, B. Chibaudel, O. Bouché, P. Hammel, Pancreatic cancer: french clinical practice guidelines for diagnosis, treatment and follow-up (SNFGE, FFCD, GERCOR, UNICANCER, SFCD, SFED, SFRO, ACHBT, AFC), Dig. Liver Dis. 50 (2018) 1257–1271, https://doi.org/10.1016/j.dld.2018.08.008.

[6] H. Yoshitomi, S. Takano, K. Furukawa, T. Takayashiki, S. Kuboki, M. Ohtsuka, Conversion surgery for initially unresectable pancreatic cancer: current status and unresolved issues, Surg. Today 49 (2019) 894–906, https://doi.org/10.1007/s00595-019-01804-x.

[7] M.J. Duffy, C. Sturgeon, R. Lamerz, C. Haglund, V.L. Holubec, R. Klapdor, A. Nicolini, O. Topolcan, V. Heinemann, Tumor markers in pancreatic cancer: a european group on tumor markers (EGTM) status report, Ann. Oncol. 21 (2009) 441–447, https://doi.org/10.1093/annonc/mdp332.

[8] U.K. Ballehaninna, R.S. Chamberlain, The clinical utility of serum CA 19-9 in the diagnosis, prognosis and management of pancreatic adenocarcinoma: an evidence based appraisal, J. Gastrointest. Oncol. 3 (2012) 105–119, https://doi.org/10.3978/j.issn.2078-6891.2011.021.

[9] B. Boekestijn, S. Feshtali, H. Vasen, M.E. van Leerdam, B.A. Bonsing, J.S.D. Mieog, M.N. Wasser, Screening for pancreatic cancer in high-risk individuals using MRI: optimization of scan techniques to detect small lesions, Fam. Cancer. 23 (2024) 295–308, https://doi.org/10.1007/s10689-024-00394-z.

[10] R.S. O'Neill, A. Stoita, Biomarkers in the diagnosis of pancreatic cancer: are we closer to finding the golden ticket? World J. Gastroenterol. 27 (2021) 4045–4087, https://doi.org/10.3748/wjg.v27.i26.4045.

[11] J.-T. Li, Y.-P. Wang, M. Yin, Q.-Y. Lei, Metabolism remodeling in pancreatic ductal adenocarcinoma, Cell Stress 3 (2019) 361–368, https://doi.org/10.15698/cst2019.12.205.

[12] S.M. El Sayed, A.A. Mahmoud, S.A. El Sawy, E.A. Abdelaal, A.M. Fouad, R. S. Yousif, M.S. Hashim, S.B. Hemdan, Z.M. Kadry, M.A. Abdelmoaty, A.G. Gabr, F. M. Omran, M.M.H. Nabo, N.S. Ahmed, Warburg effect increases steady-state ROS condition in cancer cells through decreasing their antioxidant capacities (anticancer effects of 3-bromopyruvate through antagonizing Warburg effect), Med. Hypotheses 81 (2013) 866–870, https://doi.org/10.1016/j.mehy.2013.08.024.

[13] L.-J. Su, J.-H. Zhang, H. Gomez, R. Murugan, X. Hong, D. Xu, F. Jiang, Z.-Y. Peng, Reactive oxygen species-induced lipid peroxidation in apoptosis, autophagy, and ferroptosis, Oxid. Med. Cell. Longev. 2019 (2019) 1–13, https://doi.org/10.1155/2019/5080843.

[14] J.H. Lorent, K.R. Levental, L. Ganesan, G. Rivera-Longsworth, E. Sezgin, M. Doktorova, E. Lyman, I. Levental, Plasma membranes are asymmetric in lipid unsaturation, packing and protein shape, Nat. Chem. Biol. 16 (2020) 644–652, https://doi.org/10.1038/s41589-020-0529-6.

[15] N.A. Porter, L. Xu, D.A. Pratt, Reactive sterol electrophiles: mechanisms of formation and reactions with proteins and amino acid nucleophiles, Chemistry 2 (2020) 390–417, https://doi.org/10.3390/chemistry2020025.

[16] A. Anderson, A. Campo, E. Fulton, A. Corwin, W.G. Jerome, M.S. O'Connor, 7-Ketocholesterol in disease and aging, Redox Biol. 29 (2020) 101380, https://doi.org/10.1016/j.redox.2019.101380.

[17] A. Castellaneta, I. Losito, C. Crisau, A. Zöldhegyi, Z. Hrušovská, H.-J. Rieger, I. Molnár, T.R.I. Cataldi, Overcoming challenges in LC separation of oxysterols through guided design space modelling: a comparison of three stationary phases, J. Chromatogr., A 1770 (2026) 466735, https://doi.org/10.1016/j.chroma.2026.466735.

[18] L. Iuliano, Pathways of cholesterol oxidation via non-enzymatic mechanisms, Chem. Phys. Lipids 164 (2011) 457–468, https://doi.org/10.1016/j.chemphyslip.2011.06.006.

[19] W.J. Griffiths, Y. Wang, Oxysterols as lipid mediators: their biosynthetic genes, enzymes and metabolites, Prostag. Other Lipid Mediat. 147 (2020) 106381, https://doi.org/10.1016/j.prostaglandins.2019.106381.

[20] W. Luu, L.J. Sharpe, I. Capell-Hattam, I.C. Gelissen, A.J. Brown, Oxysterols: old tale, new twists, Annu. Rev. Pharmacol. Toxicol. 56 (2016) 447–467, https://doi.org/10.1146/annurev-pharmtox-010715-103233.
[21] J. De Weille, C. Fabre, N. Bakalara, Oxysterols in cancer cell proliferation and death, Biochem. Pharmacol. 86 (2013) 154–160, https://doi.org/10.1016/j.bcp.2013.02.029.
[22] A. Spalenkova, M. Ehrlichova, S. Wei, F. Peter Guengerich, P. Soucek, Effects of 7-ketocholesterol on tamoxifen efficacy in breast carcinoma cell line models in vitro, J. Steroid Biochem. Mol. Biol. 232 (2023) 106354, https://doi.org/10.1016/j.jsbmb.2023.106354.
[23] S. Roussi, A. Winter, F. Gosse, D. Werner, X. Zhang, E. Marchioni, P. Geoffroy, M. Miesch, F. Raul, Different apoptotic mechanisms are involved in the antiproliferative effects of 7β-hydroxysitosterol and 7β-hydroxycholesterol in human colon cancer cells, Cell Death Differ. 12 (2005) 128–135, https://doi.org/10.1038/sj.cdd.4401530.
[24] A. Kloudova-Spalenkova, Y.F. Ueng, S. Wei, K. Kopeckova, F. Peter Guengerich, P. Soucek, Plasma oxysterol levels in luminal subtype breast cancer patients are associated with clinical data, J. Steroid Biochem. Mol. Biol. 197 (2020) 1–6, https://doi.org/10.1016/j.jsbmb.2019.105566.
[25] R. Lappano, A.G. Recchia, E.M. de Francesco, T. Angelone, M.C. Cerra, D. Picard, M. Maggiolini, The cholesterol metabolite 25-Hydroxycholesterol activates estrogen receptor α-Mediated signaling in cancer cells and in cardiomyocytes, PLoS One 6 (2011) e16631, https://doi.org/10.1371/journal.pone.0016631.
[26] F. Dalenc, L. Iuliano, T. Filleron, C. Zerbinati, M. Voisin, C. Arellano, E. Chatelut, P. Marquet, M. Samadi, H. Roché, M. Poirot, S. Silvente-Poirot, Circulating oxysterol metabolites as potential new surrogate markers in patients with hormone receptor-positive breast cancer: results of the OXYTAM study, J. Steroid Biochem. Mol. Biol. 169 (2017) 210–218, https://doi.org/10.1016/j.jsbmb.2016.06.010.
[27] E.R. Nelson, S.E. Wardell, J.S. Jasper, S. Park, S. Suchindran, M.K. Howe, N. J. Carver, R.V. Pillai, P.M. Sullivan, V. Sondhi, M. Umetani, J. Geradts, D. P. McDonnell, 27-Hydroxycholesterol links hypercholesterolemia and breast cancer pathophysiology, Science 342 (2013) 1094–1098, https://doi.org/10.1126/science.1241908.
[28] D. Kim, K.M. Lee, C. Lee, Y.S. Jo, M.S. Muradillaevna, J.H. Kim, J.H. Yoon, P. Song, Pathophysiological role of 27-hydroxycholesterol in human diseases, Adv. Bio. Regul. 83 (2022) 100837, https://doi.org/10.1016/j.jbior.2021.100837.
[29] I.M. Di Gangi, T. Mazza, A. Fontana, M. Copetti, C. Fusilli, A. Ippolito, F. Mattivi, A. Latiano, A. Andriulli, U. Vrhovsek, V. Pazienza, Metabolomic profile in pancreatic cancer patients: a consensusbased approach to identify highly discriminating metabolites, Oncotarget 7 (2016) 5815–5829, https://doi.org/10.18632/oncotarget.6808.
[30] M. Soncini, G. Corna, M. Moresco, N. Coltella, U. Restuccia, D. Maggioni, L. Raccosta, C.-Y.Y. Lin, F. Invernizzi, R. Crocchiolo, C. Doglioni, C. Traversari, A. Bachi, R. Bernardi, C. Bordignon, J.-Å.Å. Gustafsson, V. Russo, 24-Hydroxycholesterol participates in pancreatic neuroendocrine tumor development, Proc. Natl. Acad. Sci. 113 (2016) E6219–E6227, https://doi.org/10.1073/pnas.1613332113.
[31] H. Sadozai, A. Acharjee, H.Z. Kayani, T. Gruber, R.M. Gorczynski, B. Burke, High hypoxia status in pancreatic cancer is associated with multiple hallmarks of an immunosuppressive tumor microenvironment, Front. Immunol. 15 (2024) 1360629, https://doi.org/10.3389/fimmu.2024.1360629.
[32] W.J. Griffiths, J. Abdel-Khalik, P.J. Crick, E. Yutuc, Y. Wang, New methods for analysis of oxysterols and related compounds by LC–MS, J. Steroid Biochem. Mol. Biol. 162 (2016) 4–26, https://doi.org/10.1016/j.jsbmb.2015.11.017.
[33] N. Terrasini, V. Lionetti, Exosomes in critical illness, Crit. Care Med. 45 (2017) 1054–1060, https://doi.org/10.1097/CCM.0000000000002328.
[34] Y. Mu, M. Yang, J. Liu, Y. Yao, H. Sun, J. Zhuang, Exosomes in hypoxia: generation, secretion, and physiological roles in cancer progression, Front. Immunol. 16 (2025) 1537313, https://doi.org/10.3389/fimmu.2025.1537313.
[35] A. Botto, C. De Cesari, N. Ndimurwanko, F. Finamore, F. Greco, V. Cappello, V. Casieri, B. Immordino, V. Lionetti, M. Gemmi, I. Tonazzini, E. Giovannetti, L. A. McDonnell, Novel PPT+SEC workflow for high-sensitivity extracellular vesicle proteomics from cell media, J. Proteome Res. 24 (2025) 3129–3135, https://doi.org/10.1021/acs.jproteome.5c00082.
[36] V. Casieri, M. Matteucci, E.M. Pasanisi, A. Papa, L. Barile, R. Fritsche-Danielson, V. Lionetti, Ticagrelor enhances release of anti-hypoxic cardiac progenitor cell-derived exosomes through increasing cell proliferation in vitro, Sci. Rep. 10 (2020) 2494, https://doi.org/10.1038/s41598-020-59225-7.
[37] J.G. McDonald, D.D. Smith, A.R. Stiles, D.W. Russell, A comprehensive method for extraction and quantitative analysis of sterols and secosteroids from human plasma, J. Lipid Res. 53 (2012) 1399–1409, https://doi.org/10.1194/jlr.D022285.
[38] A. Nicoletti, M. Negri, M. Paratore, F. Vitale, M.E. Ainora, E.C. Nista, A. Gasbarrini, M.A. Zocco, L. Zileri Dal Verme, Diagnostic and prognostic role of extracellular vesicles in pancreatic cancer: current evidence and future perspectives, Int. J. Mol. Sci. 24 (2023) 885, https://doi.org/10.3390/ijms24010885.
[39] J.A. Welsh, D.C.I. Goberdhan, L. O'Driscoll, E.I. Buzas, C. Blenkiron, B. Bussolati, H. Cai, D. Di Vizio, T.A.P. Driedonks, U. Erdbrügger, J.M. Falcon-Perez, Q. Fu, A. F. Hill, M. Lenassi, S.K. Lim, M.G. Mahoney, S. Mohanty, A. Möller, R. Nieuwland, T. Ochiya, S. Sahoo, A.C. Torrecilhas, L. Zheng, A. Zijlstra, S. Abuelreich, R. Bagabas, P. Bergese, E.M. Bridges, M. Brucale, D. Burger, R.P. Carney, E. Cocucci, R. Crescitelli, E. Hanser, A.L. Harris, N.J. Haughey, A. Hendrix, A. R. Ivanov, T. Jovanovic-Talisman, N.A. Kruh-Garcia, V. Ku'ulei-Lyn Faustino, D. Kyburz, C. Lässer, K.M. Lennon, J. Lötvall, A.L. Maddox, E.S. Martens-Uzunova, R.R. Mizenko, L.A. Newman, A. Ridolfi, E. Rohde, T. Rojalin, A. Rowland, A. Saftics, U.S. Sandau, J.A. Saugstad, F. Shekari, S. Swift, D. Ter-Ovanesyan, J. P. Tosar, Z. Useckaite, F. Valle, Z. Varga, E. van der Pol, M.J.C. van Herwijnen, M. H.M. Wauben, A.M. Wehman, S. Williams, A. Zendrini, A.J. Zimmerman, C. Théry, K.W. Witwer, Minimal information for studies of extracellular vesicles (MISEV2023): from basic to advanced approaches, J. Extracell. Vesicles 13 (2024) e12404, https://doi.org/10.1002/jev2.12404.